ACS APPLIED ENERGY MATERIALS

Article

Double-layered PEDOT:PSS Films Inducing Strong Inversion Layers in Organic/Silicon Hybrid Heterojunction Solar Cells

Juye Zhu, Xi Yang, Jiang Sheng, Pingqi Gao, and Jichun Ye

ACS Appl. Energy Mater., **Just Accepted Manuscript** • DOI: 10.1021/acsaem.8b00533 • Publication Date (Web): 25 May 2018

Just Accepted

ACS Publications

is published by the American Chemical Society. 1155 Sixteenth Street N.W., Washington, DC 20036

Double-layered PEDOT:PSS Films Inducing Strong Inversion Layers in Organic/Silicon Hybrid Heterojunction Solar Cells

Juye Zhu,[a,b] Xi Yang,[a] * Jiang Sheng,[a] Pingqi Gao,[a] Jichun Ye,[a] *

Ningbo Institute of Material Technology and Engineering, Chinese Academy of Sciences, Ningbo, People's Republic of China, 315201

University of Chinese Academy of Sciences, 19 A Yuquan Rd, Shijingshan District, Beijing, People's Republic of China, 100049

*Address correspondence to yangx@nimte.ac.cn and jichun.ye@nimte.ac.cn

ABSTRACT

Poly(3,4-ethylenedioxythiophene): poly-styrenesulfonate (PEDOT:PSS) /Si hybrid heterojunction solar cells (HHSCs) have attracted wide interests due to the potential high efficiency and low-cost, but its open circuit voltage is limited. Here, double-layered PEDOT:PSS films (DL-PEDOT:PSS), high work function AI4083-type PEDOT:PSS (HW-PEDOT:PSS) used to combine with high conductivity PH1000-type PEDOT:PSS (HC-PEDOT:PSS), were applied to induce strong inversion layers at the n-type silicon surface in PEDOT:PSS/Si HHSCs resulting in quasi p-n junction. Capacitance-voltage and minority carrier lifetime mapping demonstrates that quasi p-n junction was formed by strong inversion effect with large built-in voltage. The device with DL-PEDOT:PSS with 7 wt% EG added in HW-PEDOT:PSS (EG7-DL-PEDOT:PSS) exhibits large open circuit voltage of 640 mV without any other modification, fill factor of 0.755 and power conversion efficiency of 12.69%. It suggests a promising method for the fabrication of low-cost and high-performance PEDOT:PSS/Si HHSCs, as well as p-type passivated contact in the next generation solar cells.

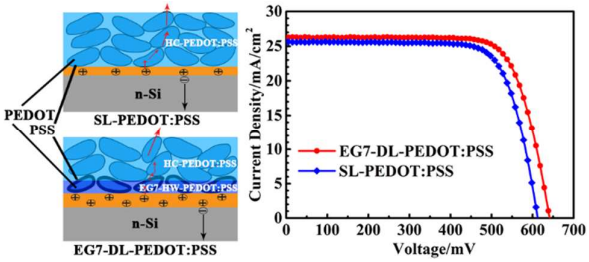

KEYWORDS: *PEDOT:PSS, hybrid heterojunction solar cells, inversion layers, additives, work function, surface passivation.*

INTRODUCTION

Hybrid heterojunction solar cells (HHSCs) comprised of Poly(3,4-ethylenedioxythiophene):poly-styrenesulfonate (PEDOT:PSS) films and n-type silicon (n-Si), have rapidly developed due to the merit of low-temperature fabrication processes (<200 ℃), uncomplicated device structure, mature crystalline silicon solar cells technology, promising power conversion efficiency (PCE) and potentially low-cost. PEDOT:PSS is deposited on the n-Si by solution-processed methods instead of the conventional diffusion process to form p-n junction, and it exhibits excellent passivation on the n-Si surface with high potential open circuit voltage (V_{OC}) of 692 mV.[1] Numerical simulation results elucidated that the PCE of the PEDOT:PSS/n-Si up to 20% could be achieved by optimizing the PEDOT:PSS layer and the device structure.[2] A mass of investigations have been carried out to improve the HHSCs performance, such as co-solvent addition,[3-5] nanostructure,[6-12] backside modification.[13-15]

For HHSCs, PEDOT:PSS as submetallic combines with n-Si forming metal/n-Si junctions without Fermi energy level pinning,[16] and induces a strong inversion layer at the silicon surface resulting in quasi p-n junction with large build-in voltage (V_{bi}), $qV_{bi} > 2|E_F\text{-}E_i|$, where E_F is the semiconductor Fermi energy level and E_i is the intrinsic Fermi energy level.[17] The main reason is that it doesn't introduce defect energy level and its excellent passivation.[18] Photo-generated carriers are harvested in the silicon and separated, and photo-generated holes are collected by PEDOT:PSS and transferred to the electrode. Consequently V_{OC} will be improved by enhancing V_{bi} through increasing the work function of PEDOT:PSS, according to $V_{bi}=\phi_m\text{-}E_F$, where ϕ_m is the metal work function. Thus, high work function materials, such as MoO_3,[19] HAT-CN,[20] were vacuum thermal evaporated over the HHSCs to increase the work function of PEDOT:PSS and improve the V_{OC}. Nevertheless, the fabrication involving vacuum system which will inevitably damage the underlying polymer film and increase

fabrication cost. While inversion layer solar cells have been demonstrated in Si-oxide systems,[21] HIT devices,[22] yielding large V_{OC} above 650 mV. Therefore, it is significant to develop facile methods to promote V_{OC}.

In this work, double-layered PEDOT:PSS films (DL-PEDOT:PSS) comprised of a high work function AI4083-type PEDOT:PSS film (HW-PEDOT:PSS) on bottom and a high conductivity PH1000-type PEDOT:PSS film (HC-PEDOT:PSS) on top, were designed to promote the V_{OC} but do not increase the series resistance of the device. They were both solution process by spin-coating. HW-PEDOT:PSS was the type of Clevios P VP AI 4083 from Heraeus with the work function of 5.0-5.2 eV,[23-25] in which the content ratio of PEDOT and PSS is 1:6. It strengthens the strong inversion layer and suppresses the surface recombination leading to larger V_{OC}. HC-PEDOT:PSS was the type of Clevios PH 1000 from Heraeus with the work function of 4.8-5.0 eV,[25-27], in which the content ratio of PEDOT and PSS is 1:2.5. The HW-PEDOT:PSS mixed with 7 wt% EG (referred as EG7-HW-PEDOT:PSS) exhibits large sheet resistance (R_{sq}, ~2.2×10^4 $\Omega\cdot sq^{-1}$), however the R_{sq} decreases sharply to 306 $\Omega\cdot sq^{-1}$ after spin-coating HC-PEDOT:PSS onto the HW-PEDOT:PSS. The influence of different mass fraction of EG added into the HW-PEDOT:PSS was investigated as well. The device with EG7-HW-PEDOT:PSS/HC-PEDOT:PSS (referred as EG7-DL-PEDOT:PSS) presents V_{OC} of 640 mV, fill factor (FF) of 0.755, short circuit current density (J_{SC}) of 26.27 mA/cm^2, and PCE of 12.69%, comparing to the conventional one with single-layered HC-PEDOT:PSS (referred as SL-PEDOT:PSS), V_{OC} of 609 mV, FF of 0.749, J_{SC} of 26.25 mA/cm^2, and PCE of 11.97%. It expresses that the DL-PEDOT:PSS with simple process enhances the work function and remains high conductivity simultaneously to further enhance V_{bi} and carriers separation, which is promising to fabricate low-cost and high performance PEDOT:PSS/Si HHSCs and be applied in the p-type passivated contact for the next generation solar cells.[28]

EXPERIMENTAL SECTION

Materials. HC-PEDOT:PSS and HW-PEDOT:PSS were two grades of PEDOT:PSS aqueous solution purchased from Heraeus, Clevios PH 1000 and Clevios P VP AI 4083, respectively. The ratio of PEDOT to PSS were 1:2.5 and 1:6 by weight, respectively. Ethylene glycol (EG) and Triton X-100 (TX) were purchased from Sigma Aldrich. All the materials were used without further purification.

Devices fabrication. N-type single-side polished Czochralski (CZ) mono-crystalline Si (100) wafers (290±10 μm) with resistivity of 0.05-0.1 Ω·cm were cleaned by RCA process. Si substrates were dipped into 10 vol% hydrofluoric acid (HF) to remove the native oxide layers, and dried by N_2. HW-PEDOT:PSS solution of Clevios P VP AI 4083 filtered through 0.45 μm filters and mixed with various mass fraction of EG and 0.1 wt% TX was spin-coated onto the Si substrates, and followed by thermal annealing at 170 ºC for 5 min to form uniform thin films about 35 nm thickness. Subsequently, HC-PEDOT:PSS solution of Clevios PH 1000 mixed with 7 wt% EG and 0.1 wt% TX was spin-coated onto the HW-PEDOT:PSS, followed by thermal annealing at 170 ℃ for 5 min. The double-layered PEDOT:PSS films and the single-layered PEDOT:PSS film were both about 90 nm thickness. The top Ag grid (6 μm thickness, 60 μm finger width, 10 mm finger length, 2 mm finger distance) electrode were formed through screen printing and Ga-In alloy was used to form ohmic contact as the rear electrode.

Characteristics. The current density-voltage (*J-V*) characteristics of devices were tested using Keithley 2400 digital source meter (Keithley, USA) under simulated sunlight illumination at 100 mW/cm^2 supplied by a xenon lamp (Oriel, USA) with AM 1.5 filter, with 1×1 cm^2 mask. The irradiation intensity was calibrated by a standard silicon photovoltaic device (Oriel, model 91150V). The temperature was accurately controlled at 25± 0.5 ℃ during the measurement. The dark *J-V* characteristics of devices were tested under dark

condition. The external quantum efficiency (EQE) system used 150 W xenon light source with a spot size of 1×2.5 mm^2 which was calibrated with a silicon photo detector from Newport. The capacitance-voltage (*C-V*) characteristics of the devices were measured by Keithley 4200-SCS Parameter Analyzer with signal frequency of 10 kHz. Surface morphology of PEDOT:PSS films were scanned by Scanning Probe Microscope (SPM; Dimension 3100). The sheet resistance of the PEDOT:PSS films with 90 nm was tested by four point probe system (Napson, Cresbox). The minority carrier lifetime was measured by minority carrier lifetime test system (WT-2000, Semilab) using microwave photoconductivity decay method, and 270±10 μm thickness n-type double-side polished Czochralski (CZ) silicon wafers with resistivity of 1-10 Ω·cm were used. PEDOT:PSS was spin-coated onto each side of the double-side silicon wafers and annealing at 170 ℃ for 10 minutes in ambient air. Reflection spectra of the PEDOT:PSS films with 90 nm spin-coated on the silicon substrates were measured by reflectivity measuring instrument (Helios LAB-rc, AudioDev GmbH) in the wavelength range of 375 nm to 1100 nm. Transmittance spectra of the PEDOT:PSS films with 90 nm coated on the quartz glass were carried out by UV/Vis/NIR spectrophotometer (Lambda 950, Perkin-Elmer) equipped with a 150-mm-diameter integrating sphere. The work function of the PEDOT:PSS films fabricated in ambient air were measured by the ultraviolet photoelectron spectroscopy (UPS, Kratos AXIS Ultra DLD) using monochromatized He I radiation (hν=21.2eV) from a He-resonance lamp.

RESULTS AND DISCUSSION

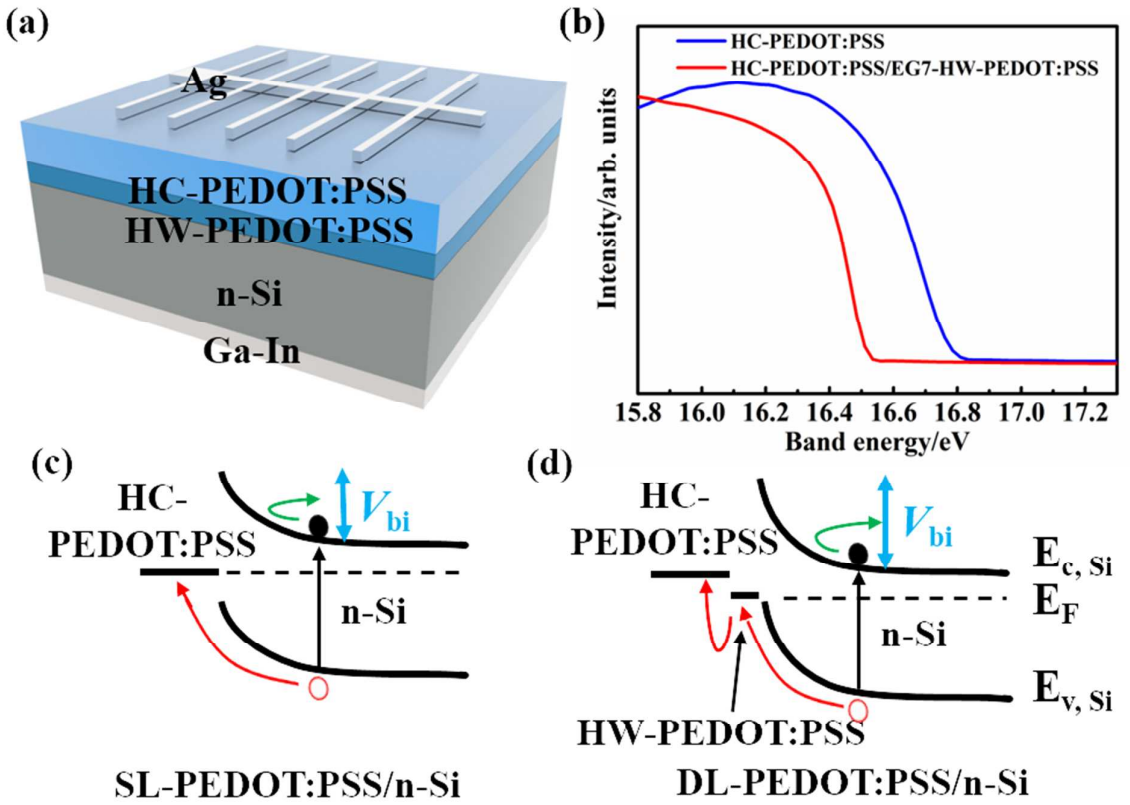

Figure 1. (a) Schematic of the devices structure. (b) Ultraviolet photoelectron spectroscopy of HC-PEDOT:PSS and HC-PEDOT:PSS/EG7-HW-PEDOT:PSS. Band energy diagrams of (c) SL-PEDOT:PSS and (d) DL-PEDOT:PSS contacting to n-Si.

Figure 1a illustrate the schematic of DL-PEDOT:PSS/Si HHSCs. PEDOT:PSS acts as submetallic and induces inversion layer at the silicon surface, forming p-n junction without doping.[16] **Figure 1**b shows the work function of PEDOT:PSS films measured by the ultraviolet photoelectron spectroscopy (UPS). HC-PEDOT:PSS and HC-PEDOT:PSS/EG7-HW-PEDOT:PSS (EG7-HW-PEDOT:PSS on the HC-PEDOT:PSS) were spin-coated on the indium-tin oxide (ITO) substrates in ambient air, which were cleaned by ethanol, acetone and isopropanol. The thickness of the films was in accord with the film thickness for devices. It shows that HC-PEDOT:PSS with work function of ~4.6 eV and HW-PEDOT:PSS with work function of ~4.8 eV, low than the previous report[24] which is mainly due to the addition of solvent[29] and the films coated in ambient air which are sensitive to the water.[30-31] It illustrates that the higher work function induces stronger inversion layer,

outputting larger V_{OC}. According to the UPS measurement, the band energy diagrams of SL-PEDOT:PSS/n-Si and DL-PEDOT:PSS/n-Si are presented in **Figure 1**c,d, respectively. In the PEDOT:PSS/Si structure, the silicide formation doesn't happen, and Fermi energy level pinning effect doesn't occur.[16] HW-PEDOT:PSS was introduced to induce stronger inversion at the n-Si surface and boost V_{bi}, leading to holes assembled at the silicon surface and reducing the recombination. However, the low conductivity HW-PEDOT:PSS didn't affect the hole transport with great tolerance to thickness of 35 nm, while the thickness of a-Si(i) in the a-Si(i)/a-Si(p) was below 10 nm.[32] The work function of the PEDOT:PSS films was tuned by adjusting the proportion of the PEDOT and PSS in the PEDOT:PSS aqueous solution.[24] The proportion of the PEDOT and PSS is 1:2.5 and 1:6 in HC-PEDOT:PSS and HW-PEDOT:PSS, respectively. HW-PEDOT:PSS introduced doesn't bring negative influence on the series resistance of the film but enhance the V_{bi}, as discussed below in detail.

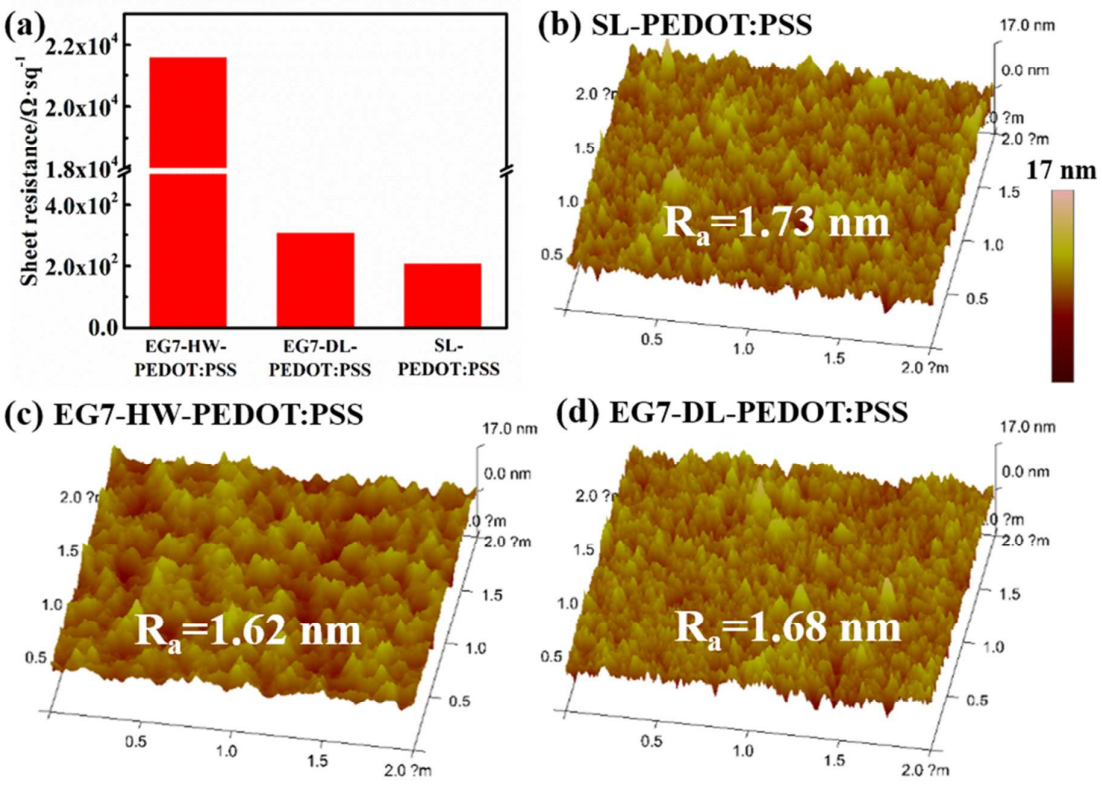

Figure 2. (a) The sheet resistance and the AFM images of (b) SL-PEDOT:PSS, (c)

EG7-HW-PEDOT:PSS, (d) EG7-DL-PEDOT:PSS. HW-PEDOT:PSS added with 7 wt% EG is referred as EG7-HW-PEDOT:PSS. HC-PEDOT:PSS coated on EG7-HW-PEDOT:PSS is referred as EG7-DL-PEDOT:PSS. Single-layered HC-PEDOT:PSS is referred as SL-PEDOT:PSS.

To evaluate the conductivity and surface structural properties of the DL-PEDOT:PSS, R_{sq} measurement and atom force microscope (AFM) were carried out. **Figure 2**a shows that the R_{sq} of the EG7-HW-PEDOT:PSS is 2.2×10^4 $\Omega\cdot sq^{-1}$. However, spin-coating HC-PEDOT:PSS onto the EG7-HW-PEDOT:PSS (referred as EG7-DL-PEDOT:PSS), R_{sq} is decreased sharply to 306 $\Omega\cdot sq^{-1}$, close to the 206 $\Omega\cdot sq^{-1}$ for the R_{sq} of SL-PEDOT:PSS. The influence of different mass fraction EG on the HW-PEDOT:PSS was investigated as well, as shown in **Figure S1**a. R_{sq} decreases from 2×10^6 $\Omega\cdot sq^{-1}$ for 0 wt%, 9.3×10^5 $\Omega\cdot sq^{-1}$ for 3 wt%, 3.7×10^5 $\Omega\cdot sq^{-1}$ for 5 wt%, 2.2×10^4 $\Omega\cdot sq^{-1}$ for 7 wt%, to 9.9×10^3 $\Omega\cdot sq^{-1}$ for 10 wt% EG added in the HW-PEDOT:PSS (referred as EG0-HW-PEDOT:PSS, EG3- HW-PEDOT:PSS, EG5-HW-PEDOT:PSS, EG7- HW-PEDOT:PSS, EG10-HW-PEDOT:PSS, respectively). It states that R_{sq} of the HW-PEDOT:PSS sharply decreases with the increasing content of EG, due to the separation and rearrangement of PEDOT chains and PSS chains and the modification of the internal crystalline ordering of individual PEDOT nanocrystals by the addition of EG, consistent with the result of the impact of the EG on the HC-PEDOT:PSS investigated by Leung et al.[5] The AFM images of the SL-PEDOT:PSS, EG7-HW-PEDOT:PSS and EG7-DL-PEDOT:PSS are shown in **Figure 2**b-d. The AFM images exhibit similar roughness (R_a) of 1.62 nm and 1.68 nm for EG7-HW-PEDOT:PSS and EG7-DL-PEDOT:PSS, respectively, close to 1.73 nm for SL-PEDOT:PSS. It shows that EG7-DL-PEDOT:PSS and SL-PEDOT:PSS exhibit similar surface morphology and EG7-HW-PEDOT:PSS doesn't affect the surface morphology.[33] **Figure S1**b-f. present the AFM images of different mass fraction of EG added into the HW-PEDOT:PSS, and the HW-PEDOT:PSS without EG

exhibits oblate ellipsoidal-shaped PEDOT-PSS core-shell structure[34] and super smooth surface characteristics with R_a of 0.72 nm. R_a increases from 0.72 nm to 2.31 nm with the increasing addition of EG from 0 wt% to 10 wt% in the HW-PEDOT:PSS. It's explained that the PEDOT chains and the PSS chains were separated and self-organized, turning from in-plane orientation to out-of-plane orientation leading to the formation of hills with large roughness after the addition of EG, which promotes carriers transporting across the PEDOT:PSS and enhance the solar cell performance. For the transmittance property, the DL-PEDOT:PSS with the addition of 0 wt%, 3 wt%, 5 wt%, 7 wt% and 10 wt% EG in the HW-PEDOT:PSS (referred as EG0-DL-PEDOT:PSS, EG3-DL-PEDOT:PSS, EG5-DL-PEDOT:PSS, EG7-DL-PEDOT:PSS, EG10-DL-PEDOT:PSS, respectively) and SL-PEDOT:PSS don't exhibit significant difference, and the transmittance of them are all above 85% in the range of 300-800 nm, as shown in **Figure S2**. It indicates that the HW-PEDOT:PSS doesn't significantly influence the sheet resistance, the surface morphology and optical property of the whole film after spin-coating HC-PEDOT:PSS onto the HW-PEDOT:PSS.

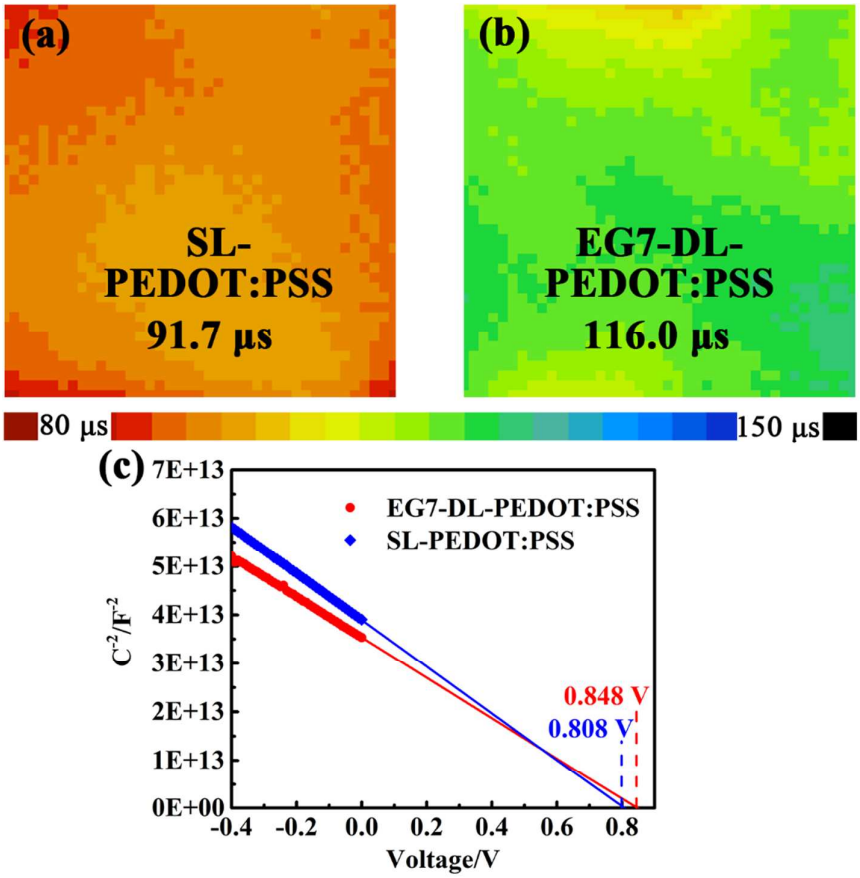

Figure 3. The minority carrier lifetime mapping images of the two-sided Si coated with (a) SL-PEDOT:PSS and (b) EG7-DL-PEDOT:PSS. (c) Capacitance vs voltage curves of PEDOT:PSS/n-Si solar cells with EG7-DL-PEDOT:PSS and SL-PEDOT:PSS.

To investigate the surface passivation quality of the DL-PEDOT:PSS on the Si, the minority carrier lifetime test was used by microwave photoconductance decay (μ-PCD) technique (WT-2000, Semilab). **Figure 3**a, b shows that the average minority carrier lifetime of the silicon wafer with 1×1 cm^2 coated with SL-PEDOT:PSS is 91.7 μs, while the average minority carrier lifetime of the silicon wafer coated with EG7-DL-PEDOT:PSS increases to 116.0 μs. According to the equation:

$$\frac{1}{\tau_{eff}} = \frac{1}{\tau_{bulk}} + \frac{2S}{W} \quad (1)$$

where τ_{eff} is the effective minority carrier lifetime, τ_{bulk} is the bulk minority carrier lifetime, S

is the surface recombination rate, and W is the wafer thickness, the larger minority carrier lifetime will reflect the lower surface recombination rate. The enhancement of the average minority carrier lifetime is attributed to the more PSS chains in EG7-HW-PEDOT:PSS than SL-PEDOT:PSS, inducing stronger field passivation, suppressing the surface recombination and keeping lower surface recombination rate. It's consistent with what found by Yaohua Mai et al. that the passivation effect was dominated by PSS species in PEDOT:PSS rather than PEDOT ones and critically sensitive to the water.[30] It elucidates that PSS passivates the Si more efficiently and the performance and stability of the HHSCs will be further improved with packaging to avoid water. The influence of different mass fraction of EG on the minority carrier lifetime was investigated as well, as shown in **Figure S3**. The minority carrier lifetime of EG0-DL-PEDOT:PSS exhibits a high value of 146.3 μs. The minority carrier lifetime decreases with the increasing mass fraction of EG, and the value of EG3-DL-PEDOT:PSS, EG5-DL-PEDOT:PSS, EG7-DL-PEDOT:PSS and EG10-DL-PEDOT:PSS is 126.6 μs, 120.0 μs, of 116.0 μs and 110.4 μs, respectively. It is mainly due to the more EG added resulting in the more void at the silicon surface.

To explore the formation of the strong inversion layer, C-V measurement was carried out, shown as plots of C^{-2}-V, exhibiting linear behavior from -0.4 V to 0 V, as shown in **Figure 3**c. Metal oxide semiconductor (MOS) capacitor model was applied to extract V_{bi}, according to the Mott-Schottky equation:

$$C^{-2} = \frac{2\left(V_{bi} - V\right)}{A^2 e\varepsilon\varepsilon_0 N_D} \quad (2)$$

where C is the capacitance, V_{bi} is the built-in potential, V is the applied voltage, A is the device area, e is the electric charge, ε is the relative dielectric constant, ε_0 is the permittivity of vacuum, and N_D is the concentration of the donor impurity. The values of V_{bi} were extracted from the extrapolation of the linear portion of the C^{-2}-V plots, which were 848 mV

for EG7-DL-PEDOT:PSS and 808 mV for SL-PEDOT:PSS, respectively, summarized in **Table 1**. It indicates that the strong inversion layer was formed.[16] The *C*-*V* curves of the device with DL-PEDOT:PSS with the different mass fraction addition of EG (from 0 wt% to 10 wt%) in the HW-PEDOT:PSS were shown in **Figure S4**a, and V_{bi} values were summarized in **Table S1**. It shows that V_{bi} of the devices slightly decreases from 855 mV to 847 mV with the increasing mass fraction addition of EG from 0 wt% to 10 wt%, but V_{bi} of the device with 5 wt% EG exhibits extremely high value of 902 mV. The extracted V_{bi} of devices with EG7-DL-PEDOT:PSS are 40 mV higher than ones with SL-PEDOT:PSS, accompanied to the increasing V_{OC} from 609 mV to 640 mV. It demonstrates that the DL-PEDOT:PSS induced stronger inversion at the silicon surface, which provided stronger driving force for carriers separation resulting in lower recombination in the depletion region.

Table 1. Photovoltaic parameters* of PEDOT:PSS/n-Si hybrid solar cells with EG7-DL-PEDOT:PSS and SL-PEDOT:PSS.

	V_{OC}/mV	J_{SC}/mA·cm^{-2}	FF	η/%	*R* at *V*oc/Ω	*R* at *I*sc/Ω	V_{bi}/mV
EG7-DL-PEDOT:PSS	**640** 637±3	**26.27** 26.42±0.28	**0.755** 0.746±0.011	**12.69** 12.55±0.14	**2.89** 3.20±0.25	**6507** 35128±50640	848
SL-PEDOT:PSS	**609** 610±2	**26.25** 25.93±0.32	**0.749** 0.748±0.004	**11.97** 11.83±0.14	**2.72** 2.84±0.24	**105122** 34728±70394	808

*Average values derived from four different datasets collected under identical conditions; Bold numbers denote maximum values.

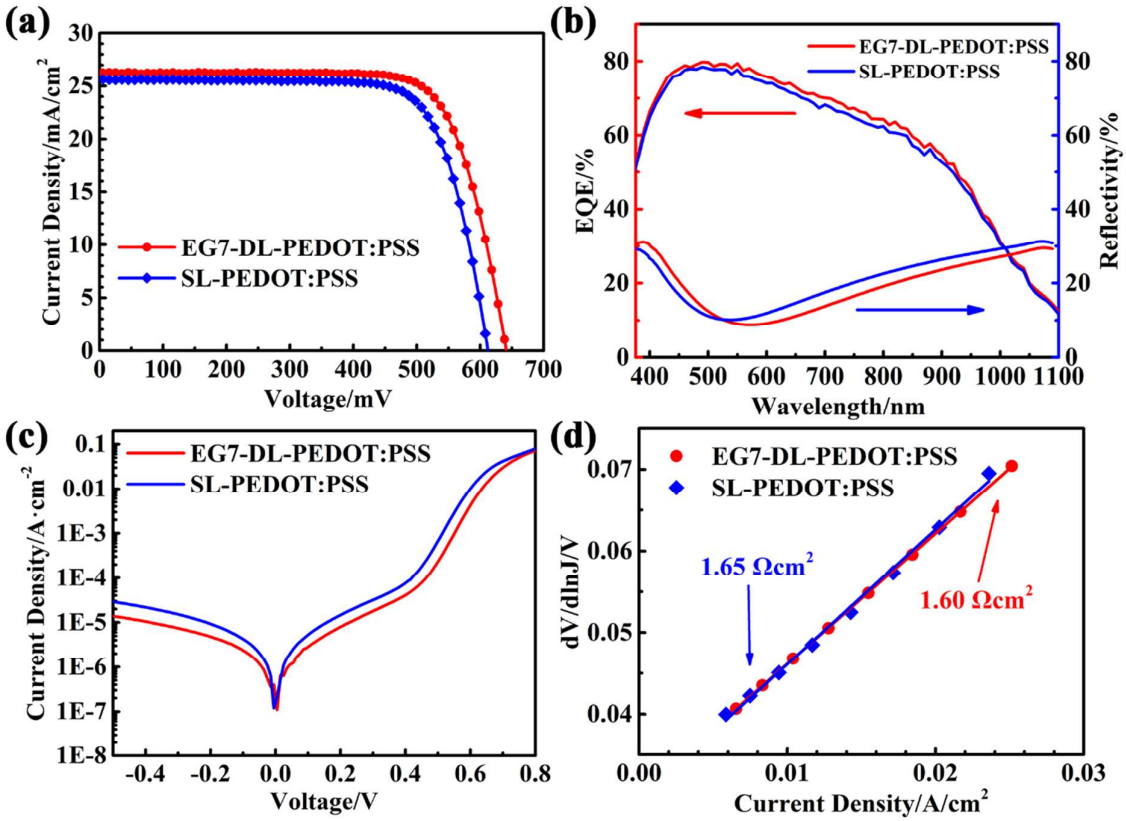

Figure 4. (a) Current density vs voltage curves, (b) EQE spectra and reflectivity spectra, (c) Dark *J-V* curves, and (d) d*V*/dln*J*-*J* curves of PEDOT:PSS/n-Si solar cells with EG7-DL-PEDOT:PSS and SL-PEDOT:PSS.

To investigate the impact of the DL-PEDOT:PSS on the performance of the PEDOT:PSS/Si HHSCs, the photovoltaic performance of the devices were measured under simulated AM 1.5 solar illumination at 100 mW·cm^{-2}. **Figure 4**a shows the current density-voltage (*J-V*) characteristics of the PEDOT:PSS/Si HHSCs with EG7-DL-PEDOT:PSS and conventional SL-PEDOT:PSS. The photovoltaic parameters were summarized in **Table 1**. It's obviously observed from the *J-V* curves that the device with EG7-DL-PEDOT:PSS presents markedly higher V_{OC} than the one with SL-PEDOT:PSS. V_{OC} of the devices with SL-PEDOT:PSS exhibits V_{OC} of 609 mV, and V_{OC} of the devices with EG7-DL-PEDOT:PSS promoted by 31 mV reaches 640 mV without any other optimizing. The short circuit current density (J_{SC}) and FF of the device with EG7-DL-PEDOT:PSS shows

26.27 mA·cm^{-2} and 0.755, and the one with SL-PEDOT:PSS exhibits similar values of 26.25 mA·cm^{-2} and 0.749. It states that the thin low conductivity EG7-HW-PEDOT:PSS doesn't increase the series resistance of the device, which will be further demonstrated by series resistance extracted from dV/dln$J$-J curves below. The device with EG7-DL-PEDOT:PSS yielded the PCE of 12.69%, comparing to the one with SL-PEDOT:PSS of 11.97%, and improved V_{OC} to 640 mV by nearly 30 mV without any other optimizing. The influence of different mass fraction EG (from 0 wt% to 10 wt%) added into the HW-PEDOT:PSS on the performance of the DL-PEDOT:PSS/Si HHSCs was investigated as well, as shown in **Figure S4**b, and the photovoltaic parameters were summarized in **Table S1**. It illustrates that J_{SC} decreased slightly from 26.96 mA·cm^{-2} for EG0-DL-PEDOT:PSS to 25.69 mA·cm^{-2} for EG10-DL-PEDOT:PSS, and FF increased from 0.692 for EG0-DL-PEDOT:PSS to 0.755 for EG7-DL-PEDOT:PSS and slightly decreased to 0.749 for EG10-DL-PEDOT:PSS. The device with EG7-DL-PEDOT:PSS exhibits the best η of 12.69% and remarkably enhancement of V_{OC} by 30 mV.

To investigate the optical property of the HHSCs, EQE spectra and reflectivity spectra were measured, as shown in **Figure 4**b. From the reflectivity spectra, it shows that the average reflectivity of the EG7-DL-PEDOT:PSS and the SL-PEDOT:PSS present 20.7% and 22.4% respectively in 400-1080 nm range. the DL-PEDOT:PSS based device displays a higher reflectance value at the short wavelength but a lower one at the long wavelength. In EQE spectra, the device with EG7-DL-PEDOT:PSS exhibits slightly gains in the whole wavelength range from 400 nm to 1100 nm comparing to the one with SL-PEDOT:PSS. The calculated J_{SC} by integrating the EQE data for the device with EG7-DL-PEDOT:PSS and SL-PEDOT:PSS is 26.82 mA/cm^2 and 26.11 mA/cm^2, respectively. The improvement in the whole wavelength range of EQE spectra for the device with DL-PEDOT:PSS is generally due to the improved junction quality resulting in effective carrier separation at the junction and

the lower reflectivity at the long wavelength.

Table 2. J_{01}, J_{02}, n_1, n_2 and R_s calculated from dark *J-V* curves for PEDOT:PSS/n-Si hybrid solar cells with EG7-DL-PEDOT:PSS and SL-PEDOT:PSS.

	J_{01}/A·cm^{-2}	J_{02}/A·cm^{-2}	n_1	n_2	R_s/Ω·cm^2
EG7-DL-PEDOT:PSS	**6.74E-11**	**1.70E-06**	**1.28**	**4.91**	**1.60**
SL-PEDOT:PSS	**3.10E-10**	**3.04E-06**	**1.32**	**4.92**	**1.65**

Figure 4c demonstrates the log*J-V* curves of devices tested in the dark condition. In the two p-n diodes model, the current equation is as follows:

$$J = J_L - J_{01}[e^{\frac{q(V-JR_s)}{n_1 kT}} - 1] - J_{02}[e^{\frac{q(V-JR_s)}{n_2 kT}} - 1] - \frac{V - JR_s}{R_{sh}} \quad (3)$$

where J_L is light current, J_{01}, J_{02} are the diode saturation current, n_1, n_2 are the ideality factors, q is the electric charge, k is Boltzmann's constant, T is the temperature, R_s is the series resistance and R_{sh} is the shunt resistance. The second and third terms of **Equation 3** describe the influence of the diodes. The different current transport mechanism is expressed by the saturation current and the ideality factor. The second term with n_1=1 at ideal state and J_{01} of proper magnitude indicates the diffusion process within the solar cell at room temperature and conforms to Shockley's diffusion theory. The third term with n_2=2 at ideal state and J_{02} generally 3 to 7 orders of magnitude larger than J_{01} indicates the recombination in the depletion region.[35] Four regimes are apparent in the forward bias region. Above 0.6 V, series resistance dominates. From 0.4 to 0.6 V, diffusion process dominates. In the 0.2-0.4 V, recombination in the depletion region dominates, and below 0.2 V, shunt resistance dominates. J_{01} and n_1 were calculated from the linear behavior in the 0.4-0.6 V, as well as J_{02} and n_2 from 0.2-0.4 V, which were summarized in **Table 2**. The conventional PEDOT:PSS/Si HHSCs with SL-PEDOT:PSS exhibits J_{01} of 3.1×10^{-10} A/cm^{-2} and J_{02} of 3.04×10^{-6} A/cm^{-2}, respectively.

For the device with EG7-DL-PEDOT:PSS, J_{01} decreases nearly 80% falling to 6.74×10^{-11} A/cm^{-2}, J_{02} falls to 1.7×10^{-6} A/cm^{-2}, n_1 falling from 1.32 for SL-PEDOT:PSS to 1.28 for EG7-DL-PEDOT:PSS and n_2 shows similar values of 4.92 for SL-PEDOT:PSS and 4.91 for EG7-DL-PEDOT:PSS, respectively. The device with EG0-DL-PEDOT:PSS shows the lowest values of J_{01} of 6.40×10^{-11} A/cm^{-2}, J_{02} of 8.57×10^{-7} A/cm^{-2} and n_1 of 1.27, but large n_2 of 5.37, due to the low recombination and the high resistance of the EG0-HW-PEDOT:PSS having an adverse effect on the carrier transport, consistent with high V_{OC} and high R_s, as shown in **Figure S5**a and summarized in **Table S2**. It illustrates that EG7-DL-PEDOT:PSS suppresses the surface recombination and improves the junction quality leading to efficient charge separation and transportation, in accordance with the minority carrier lifetime results above.

To investigate the carrier transport of the device, R_s was extracted from dark J-V,[36] as plots of dV/dln$J$-J in **Figure 4**d and summarized in **Table 2**. R_s values of the devices with EG7-DL-PEDOT:PSS and SL-PEDOT:PSS are 1.60 Ω·cm^2 and 1.65 Ω·cm^2 obtained from the slopes. It demonstrates that the insertion of the EG7-HW-PEDOT:PSS doesn't affect the series resistance of the device and the holes transport across the EG7-DL-PEDOT:PSS efficiently. However, the device with EG0-DL-PEDOT:PSS exhibits a large R_s value of as high as 5.53 Ω·cm^2, as shown in **Figure S5**b, which is due to the thick PSS shells and poor holes transport in the vertical direction. It illustrates that proper content EG added to HW-PEDOT:PSS critically reduce the sheet resistance and make no impact on the series resistance of the device.

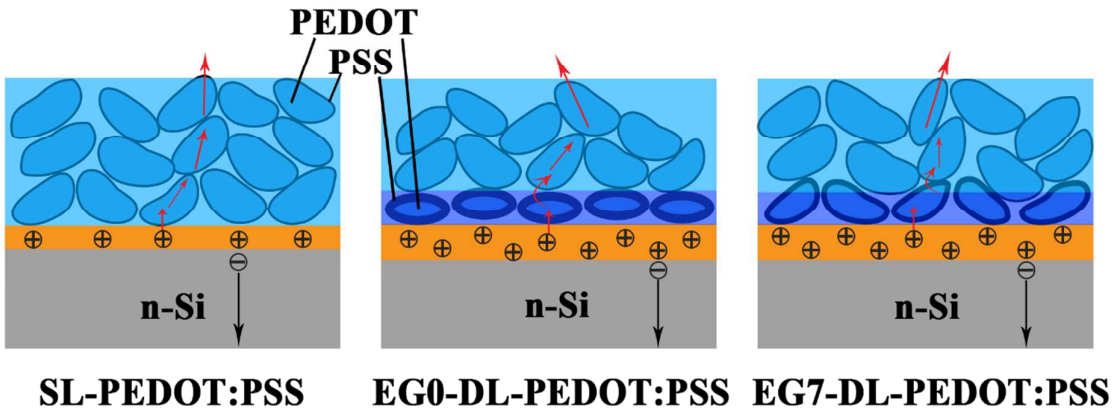

Figure 5. Diagram of carriers transport model in the PEDOT:PSS/n-Si. (left) For the SL-PEDOT:PSS, conductive PEDOT cores (blue) are surrounded by insulated PSS shells (black), inducing an inversion layer (yellow) at the silicon surface. (middle) For the EG0-DL-PEDOT:PSS, the PEDOT cores are oblate and the PSS shells are thick on the bottom HW-PEDOT:PSS layer inducing stronger inversion layer. (right) For the EG7-DL-PEDOT:PSS, the PEDOT cores are upward bended and the PSS shells are thinned on the bottom HW-PEDOT:PSS layer.

Taken all evidence together, carriers transport model was proposed in **Figure 5**. For conventional SL-PEDOT:PSS/Si, PEDOT:PSS induce an inversion layer at the silicon surface, where the photo-generated carriers separate, then electrons transport across the Si substrate and holes hop across PEDOT grains. For DL-PEDOT:PSS/Si, HW-PEDOT:PSS introduce a stronger inversion layer at the silicon surface resulting in higher hole concentration at the silicon surface. EG0-HW-PEDOT:PSS exhibits ellipsoids with thick PSS shells and fully covers Si substrate with smooth surface. EG added makes ellipsoids tip-tilted and elongated tending to vertical direction resulting in voids at the Si surface and rearranging the PEDOT chains and PSS chains making PSS shells thinner, transiting from 3D to quasi-1D variable-range-hopping (VRH) conduction which was investigated by Martijn Kemerink.[37-38] The addition of 7 wt% EG in the HW-PEDOT:PSS significantly decreases the sheet resistance and make it no negative impact on the series resistance of devices, but the tip-tilted

ellipsoids results in the formation of voids at the silicon surface, which is adverse to the passivation property and leads to the slight reduction of the minority carrier lifetime.

CONCLUSIONS

In conclusion, novel DL-PEDOT:PSS structure with HC-PEDOT:PSS on top and HW-PEDOT:PSS on bottom, was applied in PEDOT:PSS/Si HHSCs by low-temperature process to achieve quasi p-n junction. The DL-PEDOT:PSS induces the strong inversion layer at the Si surface and suppresses the Si surface recombination. Extracted from *C*-*V*, V_{bi} of the device with EG7-DL- PEDOT:PSS shows 848 mV, 40 mV larger than the one with SL-PEDOT:PSS of 808 mV. The minority carrier lifetime of EG7-DL-PEDOT:PSS and SL-PEDOT:PSS on the Si exhibits 52.9 μs and 32.3 μs, respectively. Applying EG7-DL-PEDOT:PSS, V_{OC} of the devices is substantially improved from 609 mV to 640 mV without any other modification, and series resistance of the devices doesn't increase. The device with EG7-DL-PEDOT:PSS exhibits η of 12.69% with remarkable V_{OC} of 640 mV, FF of 0.755 and J_{SC} of 26.27 mA·cm^{-2}. It gives prospects to further improve the V_{OC} by simple and low-cost solution process in the PEDOT:PSS/Si HHSCs, as well as providing a novel way to strengthen the inversion layer at the silicon surface and be applied in the p-type free-doping p-n junction or p-type passivated contact in the next generation solar cells.

ASSOCIATED CONTENT

Supporting Information

The Supporting Information is available free of charge on the ACS Publications website.

Sheet resistance and AFM images of HW-PEDOT:PSS added with different mass fraction EG; transmittance spectra of DL-PEDOT:PSS added with different mass fraction EG; minority carrier lifetime mapping images of DL-PEDOT:PSS added with different mass fraction EG; *C*-*V* curves, *J*-*V* curves, table of photovoltaic parameters of the

devices with DL-PEDOT:PSS added with different mass fraction EG; dark *J-V* curve, d*V*/dln*J-J* curve, table of J_{01}, J_{02}, n_1, n_2 of the device with EG0-DL-PEDOT:PSS.

AUTHOR INFORMATION

Corresponding Authors

*E-mail: yangx@nimte.ac.cn.

*E-mail: jichun.ye@nimte.ac.cn.

Notes

The authors declare no competing financial interest.

Acknowledgements

This work was supported by the Major State Basic Research Development Program of China (No. 2016YFB0700700), the National Natural Science Foundation of China (No. 61674154, 61404144, 61574145, 51502315, 21403262, and 51601210), the Zhejiang Provincial Natural Science Foundation (No. LR16F040002 and LY15F040003), the Major Project and Key S&T Program of Ningbo (No. 2016B10004), the Natural Science Foundation of Ningbo (No. 2017A610020 and 2017A610103).

References

(1) Schmidt, J.; Titova, V.; Zielke, D., Organic-Silicon Heterojunction Solar Cells: Open-Circuit Voltage Potential and Stability. *Appl. Phys. Lett.* **2013,** *103*, 4.

(2) Chen, T.-G.; Huang, B.-Y.; Chen, E.-C.; Yu, P.; Meng, H.-F., Micro-Textured Conductive Polymer/Silicon Heterojunction Photovoltaic Devices with High Efficiency. *Appl. Phys. Lett.* **2012,** *101*, 5.

(3) Pietsch, M.; Bashouti, M. Y.; Christiansen, S., The Role of Hole Transport in Hybrid Inorganic/Organic Silicon/Poly(3,4-ethylenedioxy-thiophene): Poly(styrenesulfonate) Heterojunction Solar Cells. *J. Phys. Chem. C* **2013,** *117*, 9049-9055.

(4) Thomas, J. P.; Leung, K. T., Defect-Minimized PEDOT:PSS/Planar-Si Solar Cell with Very High Efficiency. *Adv. Funct. Mater.* **2014,** *24*, 4978-4985.

(5) Thomas, J. P.; Zhao, L.; McGillivray, D.; Leung, K. T., High-Efficiency Hybrid Solar Cells by Nanostructural Modification in PEDOT:PSS with Co-solvent Addition. *J. Mater. Chem. A* **2014,** *2*, 2383-2389.

(6) Yu, P.; Tsai, C.-Y.; Chang, J.-K.; Lai, C.-C.; Chen, P.-H.; Lai, Y.-C.; Tsai, P.-T.; Li, M.-C.; Pan, H.-T.; Huang, Y.-Y.; Wu, C.-I.; Chueh, Y.-L.; Chen, S.-W.; Du, C.-H.; Horng, S.-F.; Meng, H.-F., 13% Efficiency Hybrid Organic/Silicon-Nanowire Heterojunction Solar Cell via Interface Engineering. *Acs Nano* **2013,** *7*, 10780-10787.

(7) Dai, X.; Chen, T.; Cai, H.; Wen, H.; Sun, Y., Improving Performance of Organic-Silicon Heterojunction Solar Cells Based on Textured Surface via Acid Processing. *ACS Appl Mater Interfaces* **2016,** *8*, 14572-7.

(8) He, J.; Yang, Z.; Liu, P.; Wu, S.; Gao, P.; Wang, M.; Zhou, S.; Li, X.; Cao, H.; Ye, J., Enhanced Electro-Optical Properties of Nanocone/Nanopillar Dual-Structured Arrays for Ultrathin Silicon/Organic Hybrid Solar Cell Applications. *Adv. Energy Mater.* **2016,** *6*, 1501793.

(9) Lee, Y.-T.; Lin, F.-R.; Chen, C.-H.; Pei, Z., A 14.7% Organic/Silicon Nanoholes Hybrid Solar Cell via Interfacial Engineering by Solution-Processed Inorganic Conformal Layer. *ACS Appl Mater Interfaces* **2016,** *8*,

34537-34545.
(10) Subramani, T.; Syu, H.-J.; Liu, C.-T.; Hsueh, C.-C.; Yang, S.-T.; Lin, C.-F., Low-Pressure-Assisted Coating Method To Improve Interface between PEDOT:PSS and Silicon Nanotips for High-Efficiency Organic/Inorganic Hybrid Solar Cells via Solution Process. *ACS Appl Mater Interfaces* **2016,** *8*, 2406-2415.
(11) Yang, Z.; Gao, P.; He, J.; Chen, W.; Yin, W.-Y.; Zeng, Y.; Guo, W.; Ye, J.; Cui, Y., Tuning of the Contact Properties for High-Efficiency Si/PEDOT:PSS Heterojunction Solar Cells. *ACS Energy Lett.* **2017,** *2*, 556-562.
(12) Jiang, Y.; Gong, X.; Qin, R.; Liu, H.; Xia, C.; Ma, H., Efficiency Enhancement Mechanism for Poly(3, 4-ethylenedioxythiophene):Poly(styrenesulfonate)/Silicon Nanowires Hybrid Solar Cells Using Alkali Treatment. *Nanoscale Res Lett* **2016,** *11*, 267.
(13) Zhang, Y.; Zu, F.; Lee, S.-T.; Liao, L.; Zhao, N.; Sun, B., Heterojunction with Organic Thin Layers on Silicon for Record Efficiency Hybrid Solar Cells. *Adv. Energy Mater.* **2014,** *4*, 1300923.
(14) Wang, D.; Sheng, J.; Wu, S.; Zhu, J.; Chen, S.; Gao, P.; Ye, J., Tuning Back Contact Property via Artificial Interface Dipoles in Si/Organic Hybrid Solar Cells. *Appl. Phys. Lett.* **2016,** *109*, 043901.
(15) Han, Y.; Liu, Y.; Yuan, J.; Dong, H.; Li, Y.; Ma, W.; Lee, S.-T.; Sun, B., Naphthalene Diimide-Based n-Type Polymers: Efficient Rear Interlayers for High-Performance Silicon-Organic Heterojunction Solar Cells. *ACS Nano* **2017,** *11*, 7215-7222.
(16) Erickson, A. S.; Zohar, A.; Cahen, D., n-Si-Organic Inversion Layer Interfaces: A Low Temperature Deposition Method for Forming a p-n Homojunction in n-Si. *Adv. Energy Mater.* **2014,** *4*, 1301724.
(17) Jackle, S.; Mattiza, M.; Liebhaber, M.; Bronstrup, G.; Rommel, M.; Lips, K.; Christiansen, S., Junction Formation and Current Transport Mechanisms in Hybrid n-Si/PEDOT:PSS Solar Cells. *Sci. Rep.* **2015,** *5*, 13008.
(18) Chen, J.; Shen, Y.; Guo, J.; Chen, B.; Fan, J.; Li, F.; Liu, H.; Xu, Y.; Mai, Y., Silicon Surface Passivation by Polystyrenesulfonate Thin Films. *Appl. Phys. Lett.* **2017,** *110*, 083904.
(19) Liu, R.; Lee, S.-T.; Sun, B., 13.8% Efficiency Hybrid Si/Organic Heterojunction Solar Cells with MoO3 Film as Antireflection and Inversion Induced Layer. *Adv. Mater.* **2014,** *26*, 6007-6012.
(20) Liu, Y.; Zhang, Z.-g.; Xia, Z.; Zhang, J.; Liu, Y.; Liang, F.; Li, Y.; Song, T.; Yu, X.; Lee, S.-t.; Sun, B., High Performance Nanostructured Silicon-Organic Quasi p-n Junction Solar Cells via Low-Temperature Deposited Hole and Electron Selective Layer. *ACS Nano* **2016,** *10*, 704-12.
(21) Godfrey, R. B.; Green, M. A., 655 mV Open-Circuit Voltage, 17.6% Efficient Silicon MIS Solar Cells. *Appl. Phys. Lett.* **1979,** *34*, 790.
(22) Taguchi, M.; Kawamoto, K.; Tsuge, S.; Baba, T.; Sakata, H.; Morizane, M.; Uchihashi, K.; Nakamura, N.; Kiyama, S.; Oota, O., HITTM Cells-High-Efficiency Crystalline Si Cells with Novel Structure. *Prog. Photovoltaics* **2000,** *8*, 503-513.
(23) Lee, T.-W.; Chung, Y.; Kwon, O.; Park, J.-J., Self-Organized Gradient Hole Injection to Improve the Performance of Polymer Electroluminescent Devices. *Adv. Funct. Mater.* **2007,** *17*, 390-396.
(24) Lee, T.-W.; Chung, Y., Control of the Surface Composition of a Conducting-Polymer Complex Film to Tune the Work Function. *Adv. Funct. Mater.* **2008,** *18*, 2246-2252.
(25) The Material Information is Available from the Heraeus Website. www.heraeus.com (accessed October).
(26) Fang, X.; Song, T.; Liu, R.; Sun, B., Two-Dimensional CoS Nanosheets Used for High-Performance Organic–Inorganic Hybrid Solar Cells. *J. Phys. Chem. C* **2014,** *118*, 20238-20245.
(27) Jackle, S.; Liebhaber, M.; Gersmann, C.; Mews, M.; Jager, K.; Christiansen, S.; Lips, K., Potential of PEDOT:PSS as a Hole Selective Front Contact for Silicon Heterojunction Solar Cells. *Sci. Rep.* **2017,** *7*, 2170.
(28) Gogolin, R.; Zielke, D.; Lövenich, W.; Sauer, R.; Schmidt, J., Silicon Heterojunction Solar Cells Combining an a-Si:H (n) Electron-Collector with a PEDOT:PSS Hole-Collector. *Energy Procedia* **2016,** *92*, 638-643.
(29) Huang, J. S.; Miller, P. F.; Wilson, J. S.; de Mello, A. J.; de Mello, J. C.; Bradley, D. D. C., Investigation of the Effects of Doping and Post-Deposition Treatments on the Conductivity, Morphology, and Work Function of Poly (3,4-ethylenedioxythiophene)/Poly (styrene sulfonate) Films. *Adv. Funct. Mater.* **2005,** *15*, 290-296.
(30) Chen, J.; Shen, Y.; Guo, J.; Chen, B.; Fan, J.; Li, F.; Liu, B.; Liu, H.; Xu, Y.; Mai, Y., Electrochemical Grafting Passivation of Silicon via Electron Transfer at Polymer/Silicon Hybrid Interface. *Electrochim. Acta* **2017,** *247*, 826-834.
(31) Koch, N.; Vollmer, A.; Elschner, A., Influence of Water on the Work Function of Conducting Poly(3,4-ethylenedioxythiophene)/Poly(styrenesulfonate). *Appl. Phys. Lett.* **2007,** *90*, 043512.
(32) Masuko, K.; Shigematsu, M.; Hashiguchi, T.; Fujishima, D.; Kai, M.; Yoshimura, N.; Yamaguchi, T.; Ichihashi, Y.; Mishima, T.; Matsubara, N.; Yamanishi, T.; Takahama, T.; Taguchi, M.; Maruyama, E.; Okamoto, S., Achievement of More than 25% Conversion Efficiency with Crystalline Silicon Heterojunction Solar Cell. *IEEE J Photovolt* **2014,** *4*, 1433-1435.
(33) Zou, Y.; Ban, M.; Cui, W.; Huang, Q.; Wu, C.; Liu, J.; Wu, H.; Song, T.; Sun, B., A General Solvent Selection Strategy for Solution Processed Quantum Dots Targeting High Performance Light-Emitting Diode. *Adv. Funct. Mater.* **2017,** *27*, 1603325.

(34) Lang, U.; Müller, E.; Naujoks, N.; Dual, J., Microscopical Investigations of PEDOT:PSS Thin Films. *Adv. Funct. Mater.* **2009,** *19*, 1215-1220.
(35) Wolf, M.; Noel, G. T.; Stirn, R. J., Investigation of the Double Exponential in the Current-Voltage Characteristics of Silicon Solar Cells. *IEEE Transactions on Electron Devices* **1977,** *24*, 419-428.
(36) Bouzidi, K.; Chegaar, M.; Aillerie, M., Solar Cells Parameters Evaluation from Dark I-V Characteristics. *Energy Procedia* **2012,** *18*, 1601-1610.
(37) Nardes, A. M.; Janssen, R. A. J.; Kemerink, M., A Morphological Model for the Solvent-Enhanced Conductivity of PEDOT:PSS Thin Films. *Adv. Funct. Mater.* **2008,** *18*, 865-871.
(38) van de Ruit, K.; Cohen, R. I.; Bollen, D.; van Mol, T.; Yerushalmi-Rozen, R.; Janssen, R. A. J.; Kemerink, M., Quasi-One Dimensional in-Plane Conductivity in Filamentary Films of PEDOT:PSS. *Adv. Funct. Mater.* **2013,** *23*, 5778-5786.

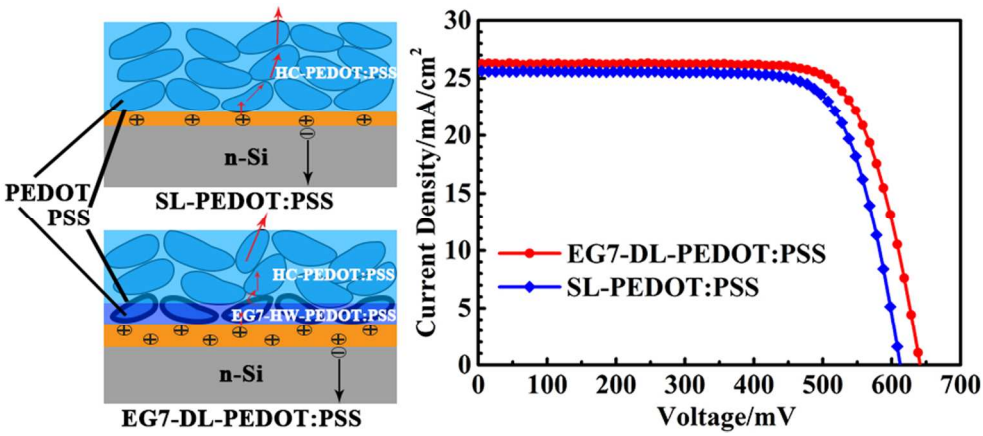

TOC

83x35mm (300 x 300 DPI)

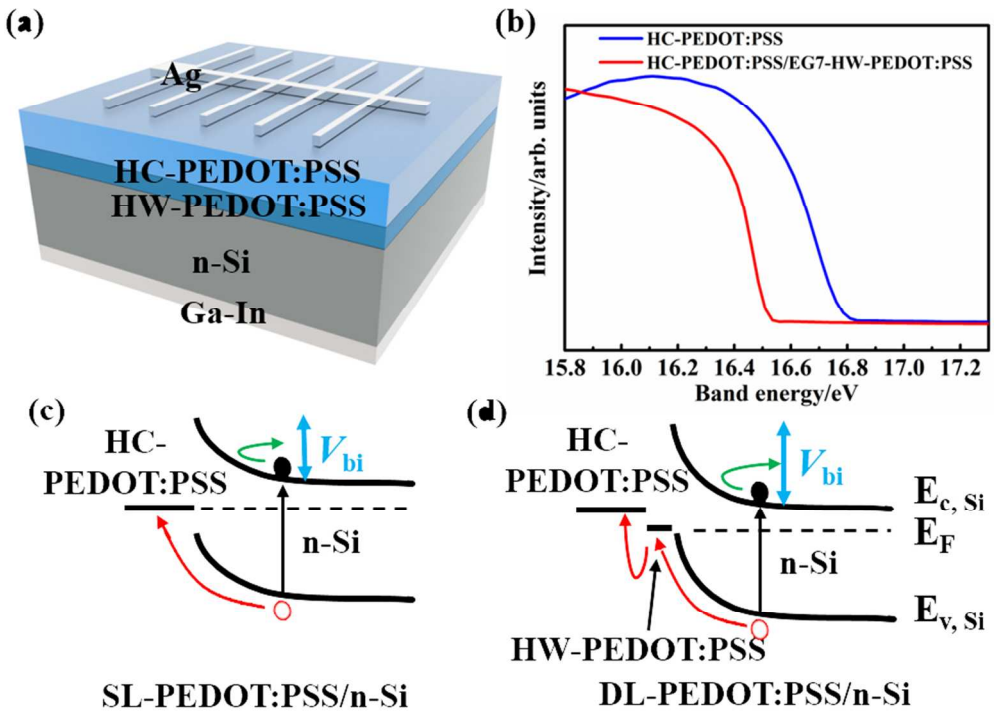

Figure 1. (a) Schematic of the devices structure. (b) Ultraviolet photoelectron spectroscopy of HC-PEDOT:PSS and HC-PEDOT:PSS/EG7-HW-PEDOT:PSS. Band energy diagrams of (c) SL-PEDOT:PSS and (d) DL-PEDOT:PSS contacting to n-Si.

165x117mm (150 x 150 DPI)

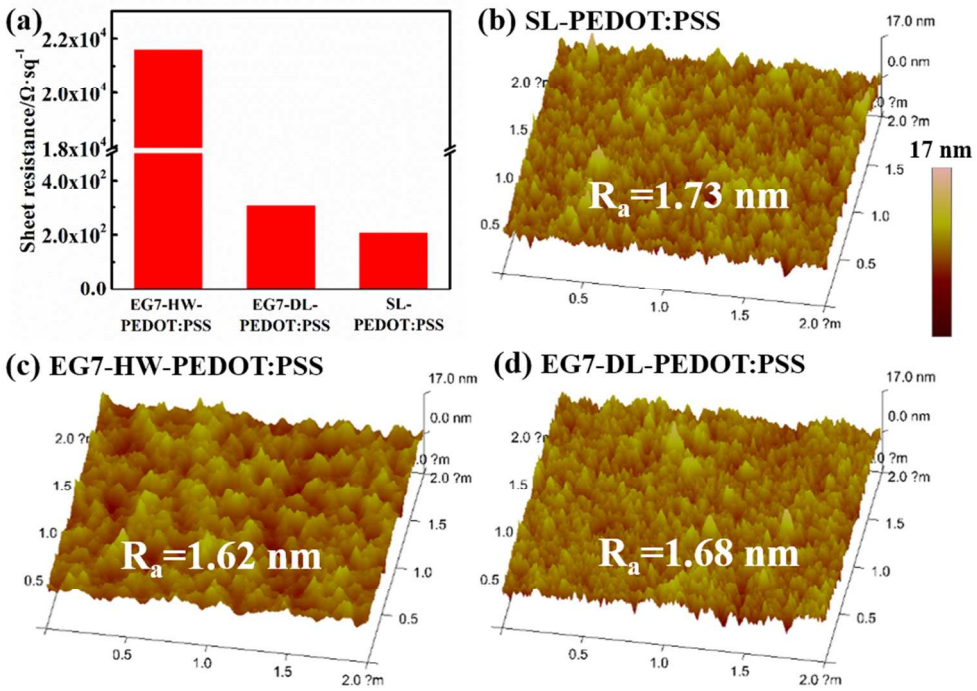

Figure 2. (a) The sheet resistance and the AFM images of (b) SL-PEDOT:PSS, (c) EG7-HW-PEDOT:PSS, (d) EG7-DL-PEDOT:PSS. HW-PEDOT:PSS added with 7 wt% EG is referred as EG7-HW-PEDOT:PSS. HC-PEDOT:PSS coated on EG7-HW-PEDOT:PSS is referred as EG7-DL-PEDOT:PSS. Single-layered HC-PEDOT:PSS is referred as SL-PEDOT:PSS.

175x123mm (300 x 300 DPI)

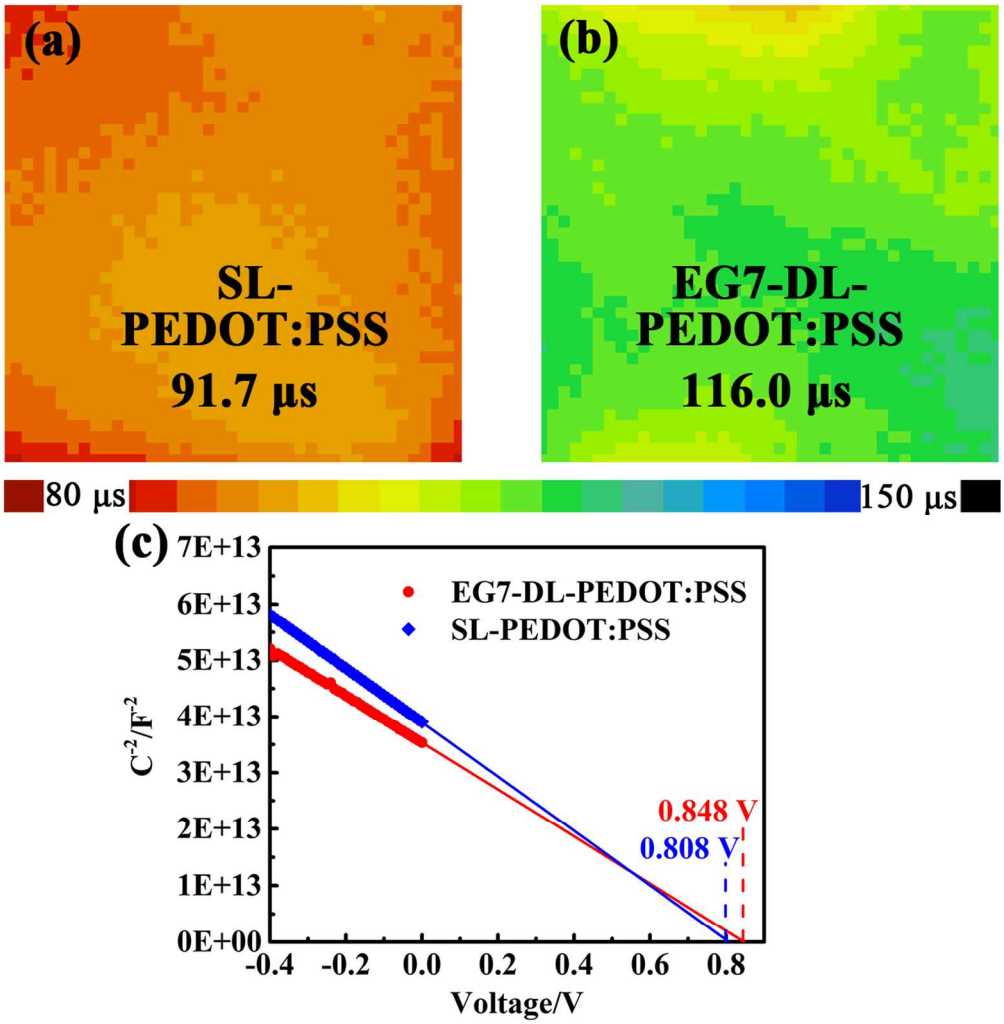

Figure 3. The minority carrier lifetime mapping images of the two-sided Si coated with (a) SL-PEDOT:PSS and (b) EG7-DL-PEDOT:PSS. (c) Capacitance vs voltage curves of PEDOT:PSS/n-Si solar cells with EG7-DL-PEDOT:PSS and SL-PEDOT:PSS.

120x123mm (300 x 300 DPI)

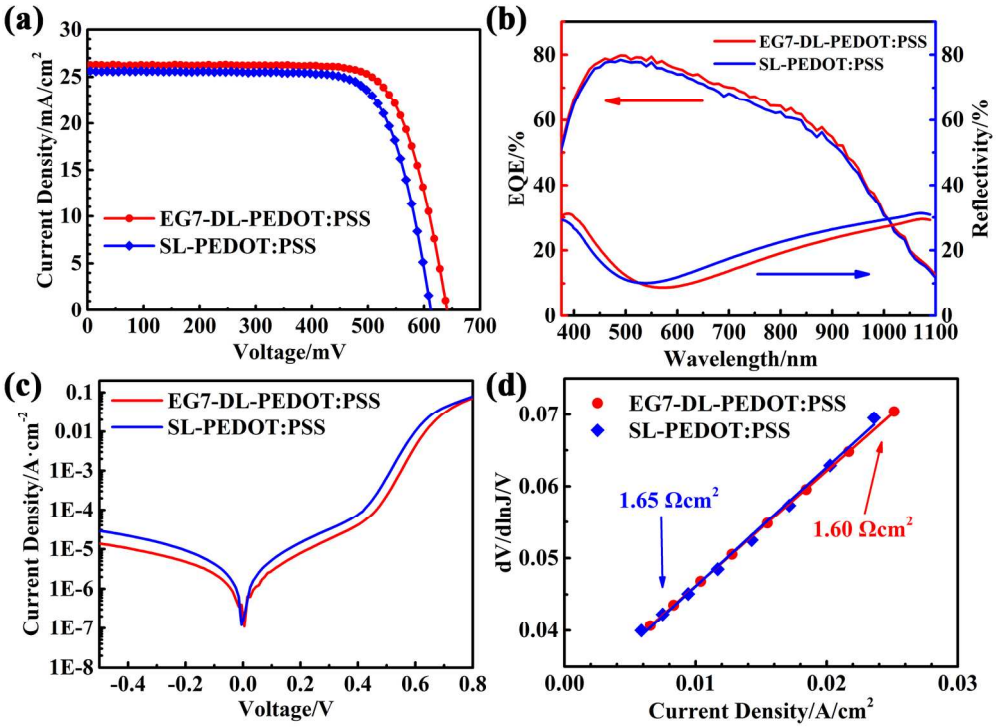

Figure 4. (a) Current density vs voltage curves, (b) EQE spectra and reflectivity spectra, (c) Dark J-V curves, and (d) dV/dlnJ-J curves of PEDOT:PSS/planar-Si solar cells with EG7-DL-PEDOT:PSS and SL-PEDOT:PSS.

173x127mm (300 x 300 DPI)

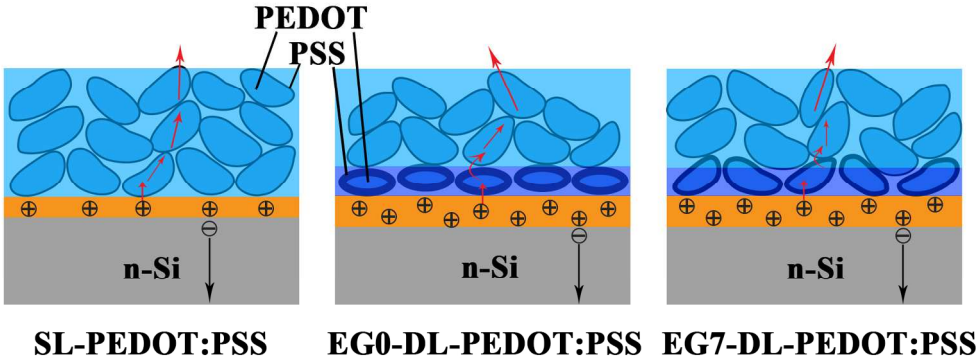

Figure 5. Diagram of carriers transport model in the PEDOT:PSS/n-Si. (left) For the SL-PEDOT:PSS, conductive PEDOT cores (blue) are surrounded by insulated PSS shells (black), inducing an inversion layer (yellow) at the silicon surface. (middle) For the EG0-DL-PEDOT:PSS, the PEDOT cores are oblate and the PSS shells are thick on the bottom HW-PEDOT:PSS layer inducing stronger inversion layer. (right) For the EG7-DL-PEDOT:PSS, the PEDOT cores are upward bended and the PSS shells are thinned on the bottom HW-PEDOT:PSS layer.

177x67mm (300 x 300 DPI)